Genomic novelty versus convergence in the basis of adaptation to whole genome duplication

Magdalena Bohutínská[1,2], Mark Alston[3], Patrick Monnahan[3], Sian Bray[3], Pirita Paajanen[3], Filip Kolář[1,2,4], and Levi Yant[5]*

1. Department of Botany, Faculty of Science, Charles University, Benátská 2, 128 01 Prague, Czech Republic
2. Institute of Botany, The Czech Academy of Sciences, Zámek 1, 252 43 Průhonice, Czech Republic
3. Department of Cell and Developmental Biology, John Innes Centre, Norwich Research Park, Norwich, NR4 7UH, UK
4. Natural History Museum, University of Oslo, Oslo, Norway
5. Future Food Beacon and School of Life Sciences University of Nottingham, Nottingham, UK

Magdalena Bohutínská and Mark Alston contributed equally.

***Author for correspondence:** levi.yant@nottingham.ac.uk; Tel: +44 7 966 731 125

Date of submission: 31 January 2020
Keywords: polyploidy; evolution; population genomics

Abstract

Whole genome duplication (WGD) occurs across kingdoms and can promote adaptation. However, the sudden increase in chromosome number, as well as immediate changes in cellular physiology, are traumatic to conserved cellular processes. Previous work in *Arabidopsis arenosa* revealed a clearly coordinated genomic response to WGD, involving a set of functionally and physically interacting proteins mediating crossover number and distribution during prophase I of meiosis. Here we ask: is this highly coordinated coevolutionary shift repeated in other species? We also test globally for convergence for all processes under selection in independent cases of adaptation to WGD, as other processes were under selection in *A. arenosa* and may be common to other independent adaptation events following WGD. Taking advantage of a well-characterised diploid/autopolyploid system, *Cardamine amara*, we test our hypothesis that convergence will be detected in the form of directional selection. We also investigate at what level convergence may be evident: identical genes, networks, or analogous processes. To do this we performed a genome scan between diploid and autotetraploid populations, while utilising a quartet-based sampling design to minimise false positives. Among the genes exhibiting the strongest signatures of selection in *C. amara* autotetraploids we detect an enrichment for DNA maintenance, chromosome organisation, and meiosis, as well as stress signalling. We find that gene-level convergence between the independent WGD adaptation events in *C. amara* and *A. arenosa* is negligible, with no more orthologous genes in common than would be expected by chance. In contrast to this, however, we observe very strong convergence at the level of functional processes and homologous (but not orthologous) genes. Taken together, our results indicate that these two autopolyploids survived the challenges attendant to WGD by modifying similar or identical processes through different molecular players and gives the first insight into the salient adaptations required to cope with a genome-doubled state.

Introduction

Whole genome duplication (WGD) is both a massive mutation and a key force in evolution[1]. The opportunities (and challenges) presented by WGD occur in an instant, realised in a single generation. As such, WGD comes as a shock to the system. Autopolyploids, formed by WGD within-species (without hybridization), emerge from the chance encounter of two sets of unreduced gametes (diploid rather than haploid). Thus, they typically harbour four full genomes that are similar in all pairwise combinations[2], resulting in a lack of pairing partner preferences at meiosis. This, combined with multiple crossover events per chromosome pair, can result in entanglements among three or more homologs at anaphase and mis-segregation or chromosome breakage, leading to aneuploidy[2–4]. Beyond this obvious challenge, WGD presents a suddenly transformed intracellular landscape to the conserved workings of the cell, such as altered ion homeostasis and a host of 'nucleotypic' factors revolving around cell size, volume, and cell cycle duration [4–6]. Occasionally however, a lineage survives this early trauma and graduates to runaway evolutionary success. Indeed there is some direct empirical evidence of the increased adaptability of polypoid lineages from in vitro evolutionary competition experiments[7]. In fact, with increased ploidy, genetic variability can be maintained in a masked state, with evidence of lineages acting as allelic sponges recruiting diverse alleles by gene flow across ploidies, and indeed, species[8,9]. Thus, while substantial opportunities may present for lineages that can adapt to a WGD state, clear challenges must be overcome to function as a polyploid[4,10,11].

The genomic basis for adaptation to WGD has been assayed in high resolution in wild, outcrossing *Arabidopsis arenosa*[12], which exists as both diploid and autotetraploid in central Europe[13]. In that case a remarkably clear signal emerged in genome scans for selective sweep following WGD: among the most extreme signals of genome-wide selection, a concerted set of highly discrete, gene-sized selective sweeps was obvious among a suite of loci that cooperatively govern meiotic chromosome crossover number and distribution during prophase I of meiosis[12,14]. The products of these genes, ASY1, ASY3, SYN1, PDS5, PRD3, ZYP1a, ZYP1b, and SMC3, physically and/or functionally interact in this tightly coordinated, conserved process, and thus represent an unusually strong candidate complex for mediating this major evolutionary transition. In the evolved autotetraploids harbouring these selected alleles, we observed a reduction in the quantity of meiotic crossovers per chromosome, relative to the rate in diploid sister lineages, and a dramatic reduction in chromosome entanglements and aneuploidy relative to synthetic autopolyploids with the diploid alleles[12].

Recent works have probed the origin of these alleles and found that in the sister species *Arabidopsis lyrata,* the autotetraploid indeed harbours the selected alleles discovered in *A. arenosa,* which again present the strongest signs of selection in *A. lyrata*[9]. Moreover, from a joint population genomic analysis of both species across a hybrid zone, clear signals of bidirectional adaptive gene flow emerge exactly at these adaptive alleles between *A. arenosa* and *A. lyrata.*[9,15] A panel of segregating populations across the hybrid zone was carefully phenotyped cytologically for meiotic chromosome configurations and the presence of each of the selected alleles was surveyed[15]. Highly contrasting single gene associations were picked up between the stability of meiosis and the presence of each of these

alleles, including a reduction in crossover number and a change in crossover distribution[15]. In seeking the origin of these adaptive alleles, both studies found that in *A. arenosa* and in *A. lyrata* there is clear signal that complementary, interacting subsets of the adaptive alleles originated in the opposite diploid species, indicating bidirectional adaptive gene flow between them. This gene flow is potentiated by the WGD itself, and thus there is an interdependence in the stabilisation of each young WGD[9,15]. Therefore, *A. lyrata* and *A. arenosa* WGD stabilisation events are not independent.

Here we use an independent system, ~17 million years diverged from both *A. arenosa* and *A. lyrata*[16], to test the hypothesis that this solution of nimble prophase I gene evolution is repeated, and if not, whether changes at other meiosis proteins are associated with adaptation to WGD. Given the clear results in the case of *A. arenosa* and *A. lyrata*, we hypothesised that the rapid changes observed in these species might be repeated, offering a striking case of repeated evolution in a core cellular process. To do this, we take advantage of a divergent[16], well-characterised diploid/autopolyploid species, *Cardamine amara* (Brassicaceae, tribe Cardamineae). A large-scale cytotyping survey and genetic structure analysis demonstrated an autopolyploid origin of the tetraploid cytotype found in the Eastern and Central Alps[17–20]. Importantly, *C. amara* occupies similar territory as both *A. arenosa* and *A. lyrata* and similar life history (perennial herb) and evolutionary history (likely single origin in the target study area, followed by tetraploid expansion associated with glacial oscillations)[18,19].

To test our hypothesis that the evolution of meiosis genes is repeated in *C. amara*, we performed a genome scan for divergent selection, contrasting natural *C. amara* tetraploid and diploid populations. We found a clear set of selection signals at genes predicted to be involved in cellular functions central to adaptation to WGD: meiosis, chromosome remodelling, cell cycle regulation, and ion transport. However, we found that *C. amara* responds to WGD very differently to *A. arenosa* and *A. lyrata*, with highly contrasting signals of selection following WGD: none of the same prophase I loci emerged as the most strongly selected genomic loci, although some homologs of those found in *A. arenosa* do exhibit signals of positive selection. Thus, we detect minimal gene-level convergence in the loci mediating prophase I meiosis adaptation. However, we find a very strong signal of process-level convergence between these two WGD adaptation events in species ~17myr diverged, indicating substantial convergence in the adaptation of core processes controlling DNA management, chromosome organisation, stress signalling, and ion homeostasis.

Results and Discussion

Population selection, sampling and genetic structure. To assess the genetic basis of adaptation to WGD in *C. amara*, we re-sequenced pools of individuals from four populations of contrasting ploidy: two diploid (LUZ, VRK) and two autotetraploid (CEZ, PIC; Fig. 1A; Table S1). We chose these populations based on a comprehensive cytological survey of over 3,000 *C. amara* samples throughout the Czech Republic[18]. The populations we sampled represent core areas of each cytotype, away from potential hybrid zones and distant from any triploid-containing populations. Further, we performed flow cytometry on all samples sequenced to verify expected ploidy.

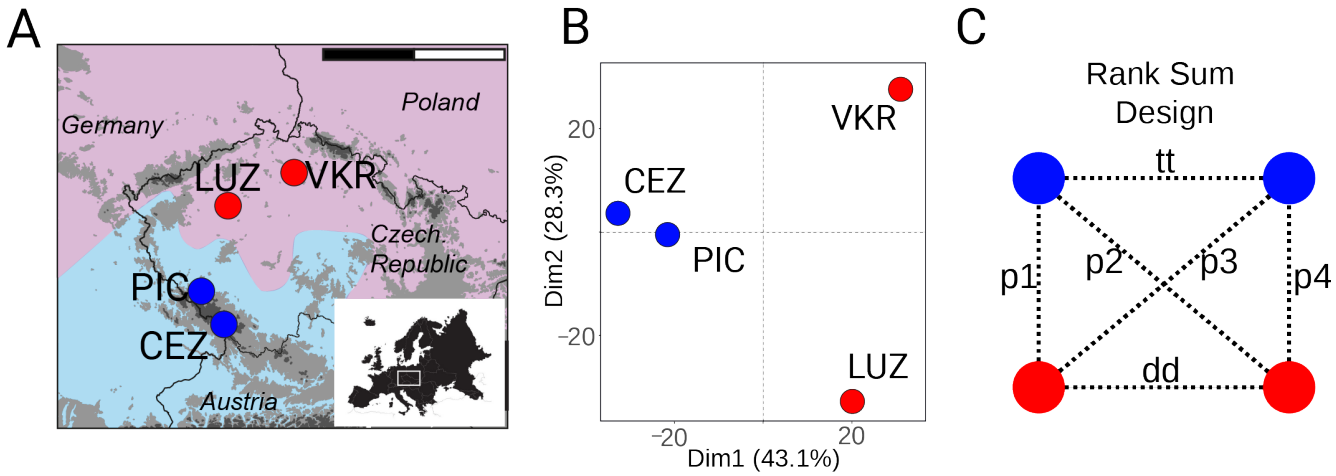

Figure 1. Sample population locations and population structure of *Cardamine amara*. **A**, Locations of *C. amara* populations sampled in the Czech Republic (red, diploids LUZ and VKR; blue, tetraploids CEZ and PIC; measure corresponds to 200 km; shaded area represents each cytotype range from [18], with evident tetraploid range expansion southward). **B**, Population structure represented by Principal Component Analysis (PCA) of ~124,000 fourfold degenerate SNPs. **C**, Rank Sum design used to minimise any influence of population-specific divergence in tests for directional selection. 'p1' to 'p4' represent the between-ploidy contrasts used for the rank sum calculations. 'dd' and 'tt' represent within-ploidy contrasts used to subtract signal of local adaptation.

To obtain robust population allele frequency estimates across the genomes, we performed a pooled sequencing approach. From each population we pooled DNA from 25 individuals in triplicate and generated on average 31 million reads per pooled sample. We mapped the reads onto our newly generated *de novo C. amara* synthetic long read assembly (n50=1.82 MB, 95% complete BUSCOs; see Methods). After read mapping, variant calling and quality filtration, we obtained a final dataset of 2,477,517 SNPs (mean coverage depth per population = 86, Table S2).

Population structure of *C. amara* represented by Principal Component Analysis (PCA) based on ~124,000 nearly neutral 4-fold degenerate (4-dg) SNPs showed primary differentiation by ploidy (first axis explained 43% of all variability) while the second axis (28% of variability explained) differentiated the two diploid populations from each other (Fig. 1B). Similarly, the two tetraploid populations had the lowest differentiation of all contrasts (Fst = 0.04, mean allele frequency difference = 0.06) and showed

a complete absence of fixed differences (Table 1). Close genetic similarity together with spatial arrangement (the populations represent part of a continuous range of tetraploid cytotype spanning to Eastern Alps) suggest that both tetraploid populations represent the outcome of a single polyploidization event, in line with previous population genetic inference based on large-scale sampling[18]. The similar level of interploidy divergence within both *C. amara* and *A. arenosa* (average Fst between diploids and tetraploids = 0.10 and 0.11, respectively) suggest that the polyploidization events in both species happened at roughly comparable time points in the past (Table 1).

Table 1. Measures of genome-wide differentiation between *C. amara* and *A. arenosa* populations

Populations	Ploidies	AFD	Fixed diff	Fst	# SNPs
PIC - VKR	4x - 2x	0.09	30	0.09	2,326,315
PIC - LUZ	4x - 2x	0.09	2	0.08	2,314,229
CEZ - VKR	4x - 2x	0.11	120	0.12	2,333,538
CEZ - LUZ	4x - 2x	0.11	86	0.11	2,335,004
CEZ - PIC	4x - 4x	0.06	0	0.04	2,297,229
LUZ - VKR	2x - 2x	0.1	6	0.09	2,018,892
arenosa diploids*	2x - 2x	-	-	0.2	-
arenosa tetraploids - arenosa diploids	4x - 2x	0.05	21	0.11	7,106,848

Note: Differentiation metrics shown are mean allele frequency difference (AFD), the number of fixed differences (Fixed diff) and Fst. *In the case of *A. arenosa,* Fst in diploids is calculated as a mean over all pairwise Fst measurements between the five characterised diploid lineages[8].

Directional selection specifically associated with WGD in *C. amara.* To minimise false positives due to local population history we leveraged a quartet-based sampling design[21], consisting of two diploid and two tetraploid populations (Fig. 1C). We calculated Fst for 1 kb windows with a minimum 20 SNPs for all six possible population contrasts, and ranked windows based on Fst values. The mean number of SNPs per population contrast was 2,270,868 (Table 1). To focus on WGD-associated adaptation, we firstly assigned ranks to each window based on the Fst values in each of four possible pairwise diploid-tetraploid contrasts and identified windows in the top 1% outliers of the resultant combined rank sum (Fig. 1C, contrasts p1-p4). We then excluded any window which was also present in the top 1% Fst outliers in diploid-diploid or tetraploid-tetraploid population contrasts to avoid misattribution caused by local population history (Fig. 1C, contrasts 'tt' and 'dd'). By this conservative approach, we identified 440 windows that intersected 229 gene coding loci (Table S3; 'candidate genes' below). Among these 229 gene coding loci, a Gene Ontology (GO) term enrichment analysis yielded 22 significantly enriched biological processes (conservative 'elim' $p < 0.05$, Table S4). To further refine the gene list to putatively functional candidates we complemented these differentiation measures with a quantitative estimate following the fineMAV method[22] (see Methods). SNPs were assigned a fineMAV score based on the predicted functional consequences of amino acid substitutions, using Grantham scores, amplified by the allele frequency difference between the two amino acids[22]. From our 229 Fst outliers, 120 contained at least one 1% fineMAV outlier amino acid substitution (Table S3, S5).

DNA maintenance (repair, chromosome organisation) and meiosis under selection in *C. amara*. Of the 22 significantly enriched GO processes, the most enriched by far was 'DNA metabolic process' (p-value = 6.50E-08, vs 0.00021 for the next most confident enrichment), although there was also enrichment for 'chromosome organization' and 'meiotic cell cycle.' The 40 genes contributing to these categories have localised peaks of differentiation (Fig. 2), as well as 1% fineMAV outlier SNPs in their gene coding regions (Table S3), indicating specifically localised selective sweeps. These genes cluster in STRING interaction networks, suggesting coevolutionary dynamics driving these selection signatures (Fig. S1; see Methods, and Results below). The largest cluster comprises of *MSH6, PDS5e, SMC2, MS5, PKL, HDA18, CRC*, and homologs of two uncharacterised, but putative DNA repair related loci *AT1G52950* and *AT3G02820* (containing SWI3 domain). *MUTS HOMOLOG 6* (*MSH6*) is a component of the post-replicative DNA mismatch repair system. It forms a heterodimer with MSH2 which binds to DNA mismatches[23,24], enhancing mismatch recognition. *MutS* homologs have also been shown to control crossover number in *A.thaliana*[25]. The *C. amara* ortholog of *AT1G15940* is a close homolog of *PDS5,* a protein required in fungi and animals for formation of the synaptonemal complex and sister chromatid cohesion[26]*. STRUCTURAL MAINTENANCE OF CHROMOSOMES 2* (*SMC2/TTN3*) is a central component of the condensin complex, which is required for segregation of homologous chromosomes at meiosis[27] and stable mitosis[28]. *PICKLE* (*PKL*) is a SWI/SWF nuclear-localized chromatin remodelling factor[29,30] that also has highly pleiotropic roles in osmotic stress response[31], stomatal aperture[32], root meristem activity[33], and flowering time[34]. Beyond this cluster, other related DNA metabolism genes among our top outliers include *DAYSLEEPER*, a domesticated transposase that is essential for plant development, first isolated as binding the *Kubox1* motif upstream of the DNA repair gene *Ku70*[35]. The complex Ku70/Ku80 regulate non-homologous end joining (NHEJ) double-strand break repair[36]. Consistent with this, *DAYSLEEPER* mutants accumulate DNA damage[37], but the exact role of *DAYSLEEPER* in normal DNA maintenance is not understood. Interesting also is the identification of *MALE-STERILE 5* (*MS5/TDM1*), which is required for cell cycle exit after meiosis II. As the name implies, MS5 mutants are male sterile, with pollen tetrads undergoing an extra round of division after meiosis II without chromosome replication[38]. *MS5/TDM1* may be an APC/C component whose function is to ensure meiosis termination at the end of meiosis II[39]. Together, this set of DNA management loci exhibiting the strongest signals of selection points to a widespread modulation of DNA repair and chromosome management following WGD in *C. amara.*

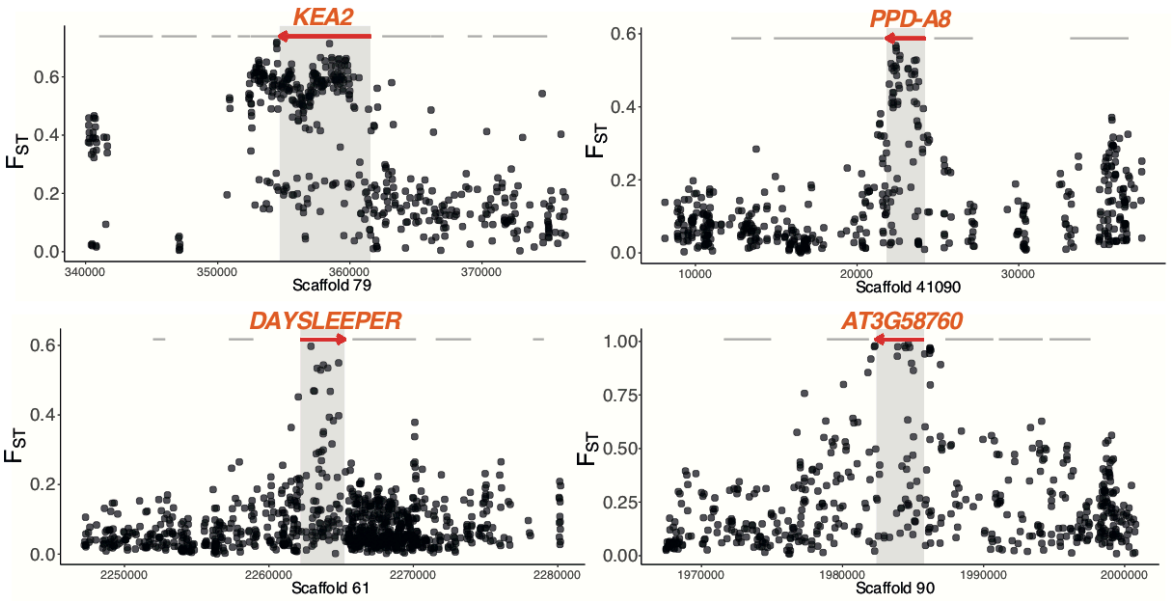

Figure 2. Selective sweep signatures at DNA management and ion homeostasis loci. Examples of selective sweep signatures among eight loci (red) among Fst candidate genes, here chosen for illustration due to inferred function or clarity of signature. X-axis gives scaffold position in base pairs. Y-axis gives Fst values at single-nucleotide polymorphisms (dots) between diploid and tetraploid *C. amara*. Red arrows indicate gene models overlapping top 1% Fst windows and grey lines indicate neighbouring gene coding loci.

Evolution of stress signalling, and ion homeostasis genes. The remainder of the enriched GO categories in *C. amara* revolved around a diversity of intracellular processes, including abiotic and biotic stress response, protein phosphorylation, root development, ABA signalling, and ion homeostasis. The intersection of these processes was often represented by several genes. For example, two of the top 20 highest-scoring SNPs in the genome-wide fineMAV analysis reside in SNF1-RELATED PROTEIN KINASE SnRK2.9 (Table S5). SnRKs have been implicated in osmotic stress and root development[40,41], and their activity also mediates the prominent roles of Clade A protein phosphatase 2C proteins in ABA and stress signalling[42]. Interesting in this respect is a strong signature of selection in *HIGHLY ABA-INDUCED PP2C GENE 1,* a clade A *PP2C* protein (Table S3). Stress-related phosphoinositide phosphatases are represented by *SAC9*, mutants of which exhibit constitutive stress responses[43].

Given the observed increase in potassium and dehydration stress tolerance in first generation autotetraploids[5], it is interesting that our window-based outliers include an especially dramatic selective sweep at *K⁺ EFFLUX ANTIPORTER 2* (*KEA2*, Fig. 2), a K^+ antiporter that modulates osmoregulation, ion, and pH homeostasis[44]. Recent evidence indicates that *KEA2* is important for eliciting a rapid hyperosmotic-induced Ca^{2+} response to water limitation imposed by osmotic stress[45]. The *KEA2* locus in autotetraploid *C. amara* features an exceptional ten fineMAV-outlier SNPs (Table S3, S5), indicating that the sweep contains a run of radical amino acid changes at high allele frequency difference between the ploidies, strongly suggesting a ploidy-selected functional change. We also detect *CATION-CHLORIDE CO-TRANSPORTER 1, HAP 5*, a Na+, K+, Cl− co-transporter, involved in diverse developmental processes and Cl− homeostasis[46].

Gene ortholog-level convergence between *C. amara* and *A. arenosa*. We hypothesized that WGD imposed strong, specific selection pressures leading to convergent directional selection on the same genes or at least on different genes playing a role in the same process (gene- or function-level convergence, respectively) between *C. amara* and *A. arenosa*. To test for this, we complemented our *C. amara* genome scan with an expanded analysis of *A. arenosa* divergence outliers based on an expanded sampling relative to the original *A. arenosa* genome scan studies[12,14]. We selected the 80 diploid and 40 tetraploid individuals sequenced most deeply in a recent range-wide survey of genomic variation in *A. arenosa* (mean coverage depth per individual = 18; 160 haploid genomes sampled of each ploidy), and scanned for Fst outliers in 1-kb-windows, as we did for *C. amara*. We identified 696 windows among 1% Fst outliers, overlapping 452 gene-coding loci (Table S6), recovering results similar to [12], including the interacting set of prophase I meiosis loci. However, from this entire list of 452 gene coding loci exhibiting signs of selective sweep following WGD in *A. arenosa*, only six orthologous loci were shared with our 229 *C. amara* Fst divergence outlier loci (Table 2). This degree of overlap is not significant (p = 0.42, Fisher's exact test), indicating no excess convergence at the level of orthologous genes. While this lack of convergence at the orthologous gene level is not a great surprise given the divergence between these two species, we note that it may at least in part be caused by the radically contrasting differences in relatedness of *C. amara* and *A. arenosa* from *A. thaliana*, the molecular model system in which the vast majority of gene function information is generated. Accordingly, *C. amara* annotations, being ~17 million years diverged from the *Arabidopsis* genus, are less certain than those for *A. arenosa*, which is three times more closely related to *A. thaliana*. This distance may obscure the true orthology between genes, making overlap at the level of functional category a stronger reflection of convergence.

Table 2. Genes under selection in both *A. arenosa* and *C. amara* following WGD

C. amara ID	A. thaliana ID	A. arenosa ID	Name	Function (TAIR)
CAg1480	*AT1G16460*	*AL1G28600*	MST2/RDH2	embryo/seed development
CAg20214	*AT2G45120*	*AL4G44210*	C2H2-like zinc finger	stress response
CAg11103	*AT3G42170*	*AL3G27110*	DAYSLEEPER	DNA repair
CAg16465	*AT3G62850*	*AL1G11960*	zinc finger-like	unknown
CAg4024	*AT5G05480*	*AL6G15370*	Asparagine amidase A	growth and development
CAg5641	*AT5G23570*	*AL6G34840*	SGS3	posttranscriptional gene silencing

Convergence by function. While we found no excess convergence at the level of orthologous genes under selection, we speculated that convergence may occur nevertheless at the level of functional pathways. To test this, we overlapped the GO terms that were significantly enriched in each species. Of the 73 enriched GO terms in *A. arenosa* (Table S7), five were identical with those enriched in the *C. amara* candidate gene list (significant overlap; p = 5.2e-06, Fisher's exact test; Table 3). In addition to this, processes related to meiosis were found in both species, but were represented by slightly different GO terms ("meiotic cell cycle" in *C. amara*, "meiotic cell cycle process" in *A. arenosa*).

Table 3. Convergent processes under selection in both *C. amara* and *A. arenosa* following WGD

GO ID	Term	p-value (C. amara)	p-value (A. arenosa)
GO:0006259	DNA metabolic process	6.50E-08	8.20E-04
GO:0051276	chromosome organization	0.019	2.10E-04
GO:0009738	abscisic acid-activated signalling pathway	0.032	0.022
GO:0071215	cellular response to abscisic acid stimulation	0.048	0.04
GO:0097306	cellular response to alcohol	0.048	0.04

Remarkably, the relative ranking of enrichments of all four convergent terms was identical in both *C. amara* and *A. arenosa* (Table 3). This stands in strong contrast to the fact that *A. arenosa* presented an obvious set of physically and functionally interacting genes in the top two categories ('DNA metabolic process' and 'chromosome organisation'), namely prophase I meiosis genes focussing on synaptonemal complex construction and function. The genes in these categories in *C. amara* appear to function in more diverse DNA management roles.

To determine whether there were other loci potentially involved in prophase I processes selected in *C. amara* that were not orthogrouped as such, we performed a search for other meiosis-related genes in *C. amara*, focussing on close homologs or gene family members that may not have been orthogrouped jointly in both species (see Methods). Several loci stand out: for example, a close homolog of the *C. amara PDS5e* exhibits the very strongest signal of selection in *A. arenosa*, *PDS5b*[12] (see Yant *et al,* 2013, Fig. 3). In addition, we note that the *C. amara* ortholog *PDS5b* harbours an unusually high three fineMAV outlier SNPs, though it is not included on the window-based candidate list. *ASY3*, which is a component of the synaptonemal complex (SC), controlling crossover distribution at meiosis, has one fineMAV outlier polymorphism. Among the other interacting prophase I genes identified under selection in *A. arenosa*, there is some evidence of selective sweep just upstream of the coding regions of *PRD3, SDS,* and *SYN1* (Table S8) in *C. amara*. Likewise, in *C. amara* we observe *SMC2-1* and in *A. arenosa*, homolog *SMC3*. Other connections across meiotic processes include the *C. amara* candidate *MS5*, regulating cell cycle number in meiosis II, which is also a functional interactor with *SMG7*[47], a top candidate in *A. arenosa* (Table S6). We note also that SMG7 exhibits elevated Fst in *C. amara*, though not as a 1% outlier (Table S8). Both act together in a pathway to facilitate exit from meiosis[47]. The key regulator of ploidy levels in *Arabidopsis* endoreduplication, *CYCA2;3*, is under selection in *A. arenosa* and is also is a 1% outlier in our *C. amara* fineMAV analysis, although it was not included in the Fst window analysis (number of SNPs < 10). However, upon inspection of Fst values of the SNPs in this gene, a window intersecting *CYCA2;3* would rank among the top 20 windows genome-wide. We note too that *PKL* (above) is also on two of the three outlier lists in *A. arenosa* ('DD' and 'CLR' outliers in Yant 2013).

Evidence for convergent protein associations. Given the tight set of physically and functionally interacting meiosis I proteins under selection in *A. arenosa*[12], we sought for evidence of such interactions in *C. amara*. Additionally, we sought for evidence that genes under selection in *C. amara* might interact with those found under selection in *A. arenosa*, which would confirm functional

convergence. Thus we took advantage of protein association information from the STRING database[48]. STRING associations are estimates of proteins' joint contributions to a shared function. While a STRING interaction does not necessarily mean that the orthologous proteins physically interact, an overabundance of such interactions among a set of proteins points to potential shared function and suggests interactions in novel systems. For each *C. amara* Fst outlier therefore we searched for the presence of STRING interactors among the *A. arenosa* Fst outliers, reasoning also that finding such associated partners under selection in two species may suggest that directional selection targeted similar functions in both species through different genes. Following this approach, we found that out of the 229 *C. amara* candidates, 90 had an associated protein among the 452 candidate genes in *A. arenosa*. In fact, 57 had more than one associated protein among *A. arenosa* candidates (Fig. 3 and Table S9). This level of overlap was greater than expected by chance (p=0.001 for both "any association" and "more-than-one association", as determined by permutation tests with the same database with 1000 randomly generated candidate lists), suggesting convergent evolution of these processes following WGD in *C. amara* and *A. arenosa.*

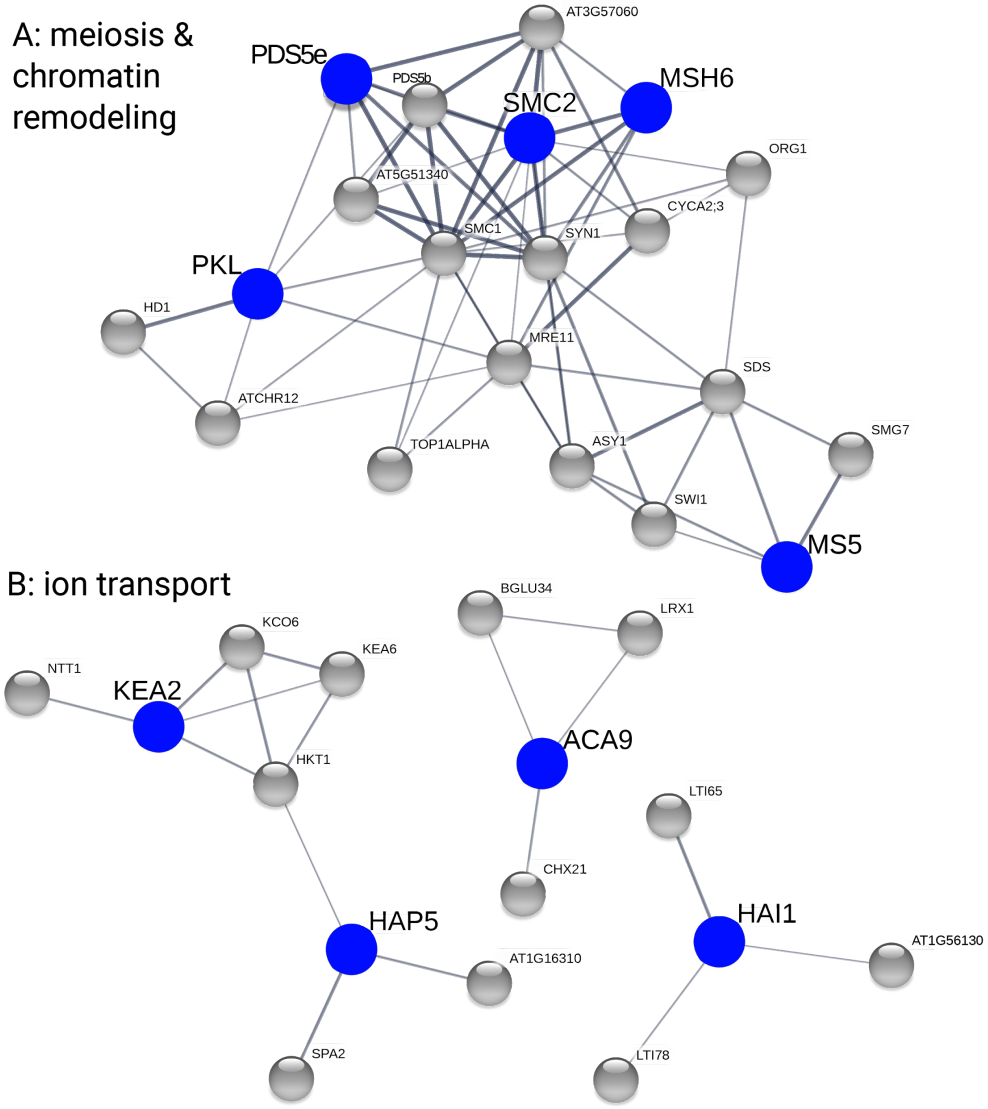

Figure 3. Evidence for functional parallelism between *C. amara* and *A. arenosa* following independent WGDs. Plots show *C. amara* candidate genes in blue and STRING-associated *A. arenosa* candidate genes in grey. We used only medium confidence associations and higher (increasing thickness of lines connecting genes indicates greater confidence). **A**, meiosis- and chromatin remodelling-related genes. **B**, ion transport- and stress-related genes.

Several large STRING clusters were evident among Fst outliers in *C. amara* and *A. arenosa* (Fig. 3). The largest of these clusters centre on genome maintenance, specifically meiosis and chromatin remodelling (Fig. 3A), and ion homeostasis (especially K+ and Ca2+), along with stress (ABA) signalling (Fig. 3B), consistent with the results of GO analysis. Taken together, both STRING and GO analyses support our hypothesis of functional convergence of these processes following WGD in *C. amara* and *A. arenosa.*

Conclusion

Given the shared challenges attendant to WGD in *C. amara* and *A. arenosa*[4,10,11], we hypothesised at least partially convergent responses in these species. While we found obvious convergent recruitment at the level of inferred functional processes, we could detect no excess convergence at orthologous genes with our genome scanning approach. This is consistent with the absence of shared standing variation between these species, being 17 million years diverged. The convergent functions (meiosis, chromosome organisation, ABA signalling, and cellular response to ABA and alcohol) provide first insights into the salient challenges associated with WGD, given that these two species are divergent evolutionary replicates. Our results detail obvious differences between the candidate solutions evolved in response to each independent WGD. Most prominent is the lack of prophase I meiosis loci under selection in *C. amara*, relative to the striking, coordinated selection of physically and functionally interacting proteins regulating crossover number and distribution in *A. arenosa*. In contrast, WGD adaptation in *C. amara* features a shift in focus to factors governing timing during later meiosis, especially the exit from meiotic divisions as evidenced by the interacting trio of *SMG7, SDS* and *MS5*, along with other chromatin remodelling factors and DNA repair-related proteins, such as *MSH6* and *DAYSLEEPER*. The biological importance of this contrast is not yet clear. It may be that *C. amara* is relatively preadapted to the challenges presented by autotetraploid crossover dynamics. Therefore, substantial reductions in crossover number mediated during prophase I may not be necessary. This could allow decoupling of the crossover reduction that dominated *A. arenosa*, from broader changes across meiosis and other processes revealed here.

Methods

Reference Genome Assembly and Alignment

We generated a *de novo* assembly using the 10x Genomics Chromium approach. In brief, a single diploid individual from pop LUZ (Table S10) was used to generate a single Chromium library, sequenced using 250PE mode on an Illumina sequencer, and assembled with Supernova version 2.0.0. This assembly had an overall scaffold N50 of 1.82mb. An assessment of genome completeness using BUSCO (version 3.0.2)[49] for the 2,251 contigs >=10kb was estimated at 94.8% (1365/1440 BUSCO groups; Table S11).

BioNano Plant Extraction protocol

Fresh young leaves of the *C. amara* accession LUZ were collected after 48-hour treatment in the dark. DNA was extracted by the Earlham Institute's Platforms and Pipelines group following an IrysPrep "Fix'n'Blend" Plant DNA extraction protocol supplied by BioNano Genomics. 2.5 g of fresh young leaves were fixed with 2% formaldehyde. After washing, leaves were disrupted and homogenized in the presence of an isolation buffer containing PVP10 and BME to prevent oxidation of polyphenols. Triton X-100 was added to facilitate the release of nuclei from the broken cells. The nuclei were then purified on a Percoll cushion. A nuclei phase was taken and washed several times in isolation buffer before embedding into low melting point agarose. Two plugs of 90 µl were cast using the CHEF Mammalian Genomic DNA Plug Kit (Bio-Rad 170-3591). Once set at 4C the plugs were added to a lysis solution containing 200 µl proteinase K (QIAGEN 158920) and 2.5 ml of BioNano lysis buffer in a 50 ml conical tube. These were put at 50C for 2 hours on a thermomixer, making a fresh proteinase K solution to incubate overnight. The 50 ml tubes were then removed from the thermomixer for 5 minutes before 50 µl RNAse A (Qiagen158924) was added and the tubes returned to the thermomixer for a further hour at 37C.The plugs were then washed 7 times in Wash Buffer supplied in Chef kit and 7 times in 1xTE. One plug was removed and melted for 2 minutes at 70C followed by 5 minutes at 43C before adding 10 µl of 0.2 U /µl of GELase (Cambio Ltd G31200). After 45 minutes at 43C the melted plug was dialysed on a 0.1 µM membrane (Millipore VCWP04700) sitting on 15 ml of 1xTE in a small petri dish. After 2 hours the sample was removed with a wide bore tip and mixed gently 5 times and left overnight at 4C.

10X library construction

DNA material was diluted to 0.5ng/ul with EB (Qiagen) and checked with a QuBit Flourometer 2.0 (Invitrogen) using the QuBit dsDNA HS Assay kit (Table S10). The Chromium User Guide was followed as per the manufacturer's instructions (10X Genomics, CG00043, Rev A). The final library was quantified using qPCR (KAPA Library Quant kit [Illumina] and ABI Prism qPCR Mix, Kapa Biosystems). Sizing of the library fragments was checked using a Bioanalyzer (High Sensitivity DNA Reagents, Agilent). Samples were pooled based on the molarities calculated using the two QC measurements. The library was clustered at 8pM with a 1% spike in of PhiX library (Illumina). The pool was run on a HiSeq2500 150bp

Rapid Run V2 mode (Illumina). The following run metrics were applied: Read 1: 250 cycles, Index 1: 8 cycles, Index 2: 0 cycles and Read 2: 250 cycles.

Sequencing and assembly and assembly QC

Raw reads were subsampled to 90 M reads and assembled with Supernova 2.0.0 (10x Genomics), giving a raw coverage of 60.30x and an effective coverage of 47.43x. The estimated molecule length was 44.15 kb. The assembly size, counting only scaffolds longer than 10kb was 159.53 Mb and the Scaffold N50 was 1.82MB. The k-mer estimate for the genome size was 225.39 MB, hence we are missing 16.61% from the assembly by retaining only contigs longer than 10Kb. We further scaffolded the assembly using the published *Cardamine hirsuta* genome using graphAlign[50] and Nucmer[51].

Gene Calling and Annotation

The "plants set" database 'embryophyta_odb9.tar.gz' was downloaded from http://busco.ezlab.org/ and used to assess orthologue presence/absence in our *C. amara* genome annotation. Running BUSCO gave Augustus[52] results via BUSCO HMMs to infer where genes lie in the assembly and returning their protein sequences. A blast (v. 2.2.4) database was built for Brassicales (taxid: 3699) by downloading ~ 1.26M protein sequences from https://www.ncbi.nlm.nih.gov/taxonomy/ and the Augustus-predicted proteins were annotated via Interproscan[53] and blast2go[54].

Orthogrouping and Reciprocal Best Blast Hits

We performed an orthogroup analysis using Orthofinder version 2.3.3[55]. to infer orthologous groups (OGs) from four species (*C. amara, A. lyrata, A. thaliana, C. pyrenaica*). A total of 21,618 OGs were found. Best reciprocal blast hits (RBHs) for *C. amara* and *A. thaliana* genes were found using BLAST version 2.9.0. *C. amara* genes were then assigned an *A. thaliana* gene ID for GO enrichment analysis via the following protocol: First, if the genes' OG contained only one *A. thaliana* gene ID, that gene ID was used. If the OG contained more than one *A. thaliana* gene, then the RBH was taken. If there was no RBH the *A. thaliana* gene ID, then the OG gene with the lowest E-value in a BLAST versus the TAIR10 database was taken. If no OG contained the *C. amara* gene, then the RBH was taken. Finally, if there was no OG or RBH then the gene with the lowest E-value in a BLAST versus the TAIR10 database was taken. BLASTs versus the TAIR10 database were performed during December 2019.

Population resequencing and genome scans

Sampling design

To isolate genomic regions subjected to directional selection acting specifically between diploids and tetraploids, we sampled a set of two diploid and two tetraploid populations (Fig. 1C). We used comparisons between populations of the same ploidy to constitute a null model for shared heterogeneity in genetic differentiation arising through processes unrelated to WGD (following an approach successfully applied in [21]).

Library preparation and sequencing

We extracted DNA in triplicate from 25 individuals for each of the following populations: CEZ (4x), PIC (4x), VKR (2x), and LUZ (2x). All plants used for DNA extraction were verified for expected ploidy by flow cytometry. We then pooled samples of each population, constructed Illumina Truseq libraries (Illumina), and sequenced them on Illumina's NextSeq platform at a 150 base pair, paired-end specification.

Data preparation, alignment, and genotyping

Fastq files from the two runs were combined and concatenated to give an average of 30.5 million reads per sample (see 'sample_read_counts.xlsx'). Adapter sequences were removed via the cutadapt software (version 1.9.1)[56] and quality trimmed via Sickle (version 33)[57] to generate only high-quality reads (Phred score >=30) of 30bp or more, resulting in an average of 27.9 million reads per sample. Using samtools (v. 1.7)[58] and bwa (v. 0.7.12)[59] software, the quality-filtered reads were aligned against two references: 89.3% of reads mapped to our *C. amara* assembly, while only 74.5% to *C. hirsuta*. We retained only the alignment to *C. amara* for all analysis. Using the picard software tool (v. 1.134)[60], first duplicate reads were removed via 'MarkDuplicates' followed by the addition of read group IDs to the bam files via 'AddOrReplaceReadGroups'. Finally, to handle the presence of indels, GATK (v. 3.6.0)[61] was used to realign reads to the *C. amara* assembly via 'RealignerTargetCreator' and 'IndelRealigner'.

Variant Calling

Text files describing sample populations and ploidy were prepared, and variants called for the 12 bam files using Freebayes (v. 1.1.0.46)[62] to generate a single VCF output. Due to working with pooled (high ploidy) samples, Freebayes was run with '--pooled-discrete' (assumes samples result from pooled sequencing). In addition, the software was restricted to biallelic sites ('--use-best-n-alleles 2') and indel sites were excluded ('--no-indels'). The VCF was filtered via bcftools (v 1.8)[63] to remove sites where the read depth was < 10 or greater than 1.6x the second mode (determined as 1.6 x 31 = 50, Fig. S2).

Population genetic structure

We first calculated genome-wide between-population metrics (Nei's Fst[64] and allele frequency difference). We calculated allele frequencies (AF) as the average AF of all the pools. The AF in individual pools has been calculated as the fraction of the total number of reads supporting the alternative allele[65]. We used the python3 PoolSeqBPM pipeline, designed to input pooled data (https://github.com/mbohutinska/PoolSeqBPM). Then we inferred relationships between populations as genetic distances using principal component analysis (PCA) implemented in *adegenet*[66].

Window-based selection scan using a quartet design

We performed a window-based Fst (Nei) scan for directional selection in *C. amara*, taking advantage of quartet of two diploid and two tetraploid populations (Fig. 1C). Using such quartet design, we identified top candidate windows for selective sweeps associated with ploidy differentiation, while excluding differentiation patterns private to a single population or ploidy-uninformative selective

sweeps. To do so, we calculated Fst for 1 kb windows with minimum 20 SNPs for all six population pairs in the quartet (Fig. 1C) and ranked windows based on their Fst value. We excluded windows which were top 1% outliers in diploid-diploid (dd in Fig. 1C) or tetraploid-tetraploid (tt) populations contrasts, as they represent variation inconsistent with diploid-tetraploid divergence but rather signal local differentiation within a cytotype. Next, we assigned ranks to each window based on the Fst values in four diploid-tetraploid contrasts and identified windows being top 1% outliers of minimum rank sum.

To account for possible confounding effect of comparing windows from genic and non-genic regions, we calculated the number of base pairs overlapping with any gene within each window. There was not any relationship between the proportion of genic space within a window and Fst (Fig. S3), indicating that our analyses were unaffected by unequal proportion of genic space in a window.

In *A. arenosa*, we performed window-based Fst scan for directional selection using the same criteria as for *C. amara* (1kb windows, min 20 SNPs per window). We did not use the quartet design as the range-wide dataset of 80 diploid and 40 tetraploid individuals drawn from many popultions assured power to detect genomic regions with WGD-associated differentiation.

fineMAV

We downloaded coding sequences from the *C. hirsuta* genomic resources web site *http://chi.mpipz.mpg.de/download/annotations/carhr38.cds.*fa and mapped to *C. amara* using gmap. The resulting sam file was converted to bam-format, sorted and indexed via samtools (v. 1.7)[58], and then converted to GTF-format via the 'convert' script in Mikado (v1.2.3)[67] which was subsequently used to build a snpEFF (v. 4.3)[68] database. We overlapped the candidate minimum rank sum SNPs with candidate SNPs from fineMAV analysis and annotated each SNP identified by both methods with gene to which it belongs. The top candidate gene was annotated to the corresponding molecular network using the software SIFT[68].

GO enrichment analysis

To infer functions significantly associated with directional selection following WGD, we performed gene ontology enrichment of gene list using the R package topGO[69], using *A. thaliana* orthologs of *C. amara/A. lyrata* genes, obtained using biomaRt[70]. We used Fisher's exact test with conservative 'elim' method, which tests for enrichment of terms from the bottom of the GO hierarchy to the top and discards any genes that are significantly enriched in a descendant GO terms[71]. We used 'biological process' ontology with minimum node size 150 genes.

Protein associations from STRING database.

We searched for association among *C. amara* and *A. arenosa* candidate genes using STRING[48] database. We used multiple proteins search in *A. thaliana*, with text mining, experiments, databases, co-expression, neighbourhood, gene fusion and co-occurrence as information sources. We used minimum confidence 0.4 and retained only 1st shell associations.

Quantifying convergence

We considered convergent candidates all candidate genes or significantly enriched GO categories that overlapped across both species. Convergent candidate genes had to be members of the same orthogroups[55]. To test for higher than random number of overlapping items we used Fisher's Exact Test for Count Data in R[72].

Data Availability

All sequence data are freely available in the European Nucleotide Archive (ENA; https://www.ebi.ac.uk/ena) and will be available upon publication.

Acknowledgements

The authors thank Veronika Konečná for assistance with the map figure. This work was supported by the European Research Council (ERC) under the European Union's Horizon 2020 research and innovation programme [grant number ERC-StG 679056 HOTSPOT], via a grant to LY. Additional support was provided by Czech Science Foundation (project 20-22783S to FK).

Author Contributions

LY conceived the study. MB, MA, PP, SB and PM performed analyses. PM performed laboratory experiments. FK, SB, and PM performed field collections. LY and MB wrote the manuscript with input from all authors. All authors approved of the final manuscript.

Competing Interests statement

The authors declare no competing interests.

Materials & Correspondence

All requests should be addressed to Levi Yant at levi.yant@nottingham.ac.uk

References

1. Van De Peer, Y., Mizrachi, E. & Marchal, K. The evolutionary significance of polyploidy. *Nature Reviews Genetics* vol. 18 411–424 (2017).
2. Lloyd, A. & Bomblies, K. Meiosis in autopolyploid and allopolyploid Arabidopsis. *Current Opinion in Plant Biology* vol. 30 116–122 (2016).
3. Bomblies, K. & Madlung, A. Polyploidy in the Arabidopsis genus. *Chromosome Research* vol. 22 117–134 (2014).
4. Yant, L. & Bomblies, K. Genome management and mismanagement—cell-level opportunities and challenges of whole-genome duplication. *Genes Dev.* **29**, 2405–2419 (2015).
5. Chao, D. Y. *et al.* Polyploids exhibit higher potassium uptake and salinity tolerance in Arabidopsis. *Science (80-.).* **341**, 658–659 (2013).
6. Doyle, J. J. & Coate, J. E. Polyploidy, the nucleotype, and novelty: The impact of genome doubling on the biology of the cell. *International Journal of Plant Sciences* vol. 180 1–52 (2019).
7. Selmecki, A. M. *et al.* Polyploidy can drive rapid adaptation in yeast. *Nature* **519**, 349–351 (2015).
8. Monnahan, P. *et al.* Pervasive population genomic consequences of genome duplication in Arabidopsis arenosa. *Nat. Ecol. Evol.* **3**, 457–468 (2019).
9. Marburger, S. *et al.* Interspecific introgression mediates adaptation to whole genome duplication. *Nat. Commun.* (2019) doi:10.1038/s41467-019-13159-5.
10. Bomblies, K., Higgins, J. D. & Yant, L. Meiosis evolves: Adaptation to external and internal environments. *New Phytol.* **208**, 306–323 (2015).
11. Baduel, P., Bray, S., Vallejo-Marin, M., Kolář, F. & Yant, L. The 'Polyploid Hop': Shifting challenges and opportunities over the evolutionary lifespan of genome duplications. *Front. Ecol. Evol.* **6**, (2018).
12. Yant, L. *et al.* Meiotic adaptation to genome duplication in Arabidopsis arenosa. *Curr. Biol.* **23**, 2151–2156 (2013).
13. Kolář, F. *et al.* Northern glacial refugia and altitudinal niche divergence shape genome-wide differentiation in the emerging plant model Arabidopsis arenosa. *Mol. Ecol.* (2016) doi:10.1111/mec.13721.
14. Hollister, J. D. *et al.* Genetic Adaptation Associated with Genome-Doubling in Autotetraploid Arabidopsis arenosa. *PLoS Genet.* **8**, (2012).
15. Seear, P. J. *et al.* A novel allele of ASY3 promotes meiotic stability in autotetraploid Arabidopsis lyrata. *bioRxiv* 2019.12.25.888388 (2019) doi:10.1101/2019.12.25.888388.
16. Huang, X. C., German, D. A. & Koch, M. A. Temporal patterns of diversification in Brassicaceae demonstrate decoupling of rate shifts and mesopolyploidization events. *Ann. Bot.* **125**, 29–47 (2020).
17. Lihová, J., Aguilar, J. F., Marhold, K. & Feliner, G. N. Origin of the disjunct tetraploid Cardamine amporitana (Brassicaceae) assessed with nuclear and chloroplast DNA sequence data. *Am. J. Bot.* **91**, 1231–1242 (2004).
18. Zozomová-Lihová, J. *et al.* Cytotype distribution patterns, ecological differentiation, and genetic structure in a diploid– tetraploid contact zone of Cardamine amara. *Am. J. Bot.* **102**, 1380–1395 (2015).
19. Marhold, K., Huthmann, M. & Hurka, H. Evolutionary history of the polyploid complex of Cardamine amara (Brassicaceae): isozyme evidence. *Plant Syst. Evol.* **233**, 15–28 (2002).
20. Marhold, K. Taxonomic evaluation of the tetraploid populations of Cardamine amara

(Brassicaceae) from the Eastern Alps and adjacent areas. *Bot. Helv.* **109**, 67–84 (1999).

21. Vijay, N. *et al.* Evolution of heterogeneous genome differentiation across multiple contact zones in a crow species complex. *Nat. Commun.* **7**, (2016).
22. Szpak, M. *et al.* FineMAV: Prioritizing candidate genetic variants driving local adaptations in human populations. *Genome Biol.* **19**, (2018).
23. Culligan, K. M. & Hays, J. B. Arabidopsis MutS homologs - AtMSH2, AtMSH3, AtMSH6, and a novel AtMSH7 - Form three distinct protein heterodimers with different specificities for mismatched DNA. *Plant Cell* **12**, 991–1002 (2000).
24. Wu, S. Y., Culligan, K., Lamers, M. & Hays, J. Dissimilar mispair-recognition spectra of Arabidopsis DNA-mismatch-repair proteins MSH2·MSH6 (MutSα) and MSH2·MSH7 (MutSγ). *Nucleic Acids Res.* **31**, 6027–6034 (2003).
25. Lu, X. *et al.* The Arabidopsis MutS homolog AtMSH5 is required for normal meiosis. *Cell Res.* **18**, 589–599 (2008).
26. Panizza, S., Tanaka, T., Hochwagen, A., Eisenhaber, F. & Nasmyth, K. Pds5 cooperates with cohesion in maintaining sister chromatid cohesion. *Curr. Biol.* **10**, 1557–1564 (2000).
27. Siddiqui, N. U., Stronghill, P. E., Dengler, R. E., Hasenkampf, C. A. & Riggs, C. D. Mutations in Arabidopsis condensin genes disrupt embryogenesis, meristem organization and segregation of homologous chromosomes during meiosis. *Development* **130**, 3283–3295 (2003).
28. Liu, C. M. & Meinke, D. W. The titan mutants of Arabidopsis are disrupted in mitosis and cell cycle control during seed development. *Plant J.* **16**, 21–31 (1998).
29. Shaked, H., Avivi-Ragolsky, N. & Levy, A. A. Involvement of the arabidopsis SWI2/SNF2 chromatin remodeling gene family in DNA damage response and recombination. *Genetics* **173**, 985–994 (2006).
30. Ogas, J., Kaufmann, S., Henderson, J. & Somerville, C. PICKLE is a CHD3 chromatin-remodeling factor that regulates the transition from embryonic to vegetative development in Arabidopsis. *Proc. Natl. Acad. Sci. U. S. A.* **96**, 13839–13844 (1999).
31. Perruc, E., Kinoshita, N. & Lopez-Molina, L. The role of chromatin-remodeling factor PKL in balancing osmotic stress responses during Arabidopsis seed germination. *Plant J.* **52**, 927–936 (2007).
32. Kang, X. *et al.* HRB2 and BBX21 interaction modulates Arabidopsis ABI5 locus and stomatal aperture. *Plant Cell Environ.* **41**, 1912–1925 (2018).
33. Aichinger, E., Villar, C. B. R., di Mambro, R., Sabatini, S. & Köhler, C. The CHD3 chromatin remodeler PICKLE and polycomb group proteins antagonistically regulate meristem activity in the Arabidopsis root. *Plant Cell* **23**, 1047–1060 (2011).
34. Jing, Y., Guo, Q. & Lin, R. The Chromatin-Remodeling Factor PICKLE Antagonizes Polycomb Repression of FT to Promote Flowering. *Plant Physiol.* **181**, 656–668 (2019).
35. Bundock, P. & Hooykaas, P. An Arabidopsis hAT-like transposase is essential for plant development. *Nature* **436**, 282–284 (2005).
36. Tamura, K., Adachi, Y., Chiba, K., Oguchi, K. & Takahashi, H. Identification of Ku70 and Ku80 homologues in Arabidopsis thaliana: Evidence for a role in the repair of DNA double-strand breaks. *Plant J.* **29**, 771–781 (2002).
37. Knip, M. (Leiden U. Daysleeper : from genomic parasite to indispensable gene. (2012).
38. Glover, J., Grelon, M., Craig, S., Chaudhury, A. & Dennis, E. Cloning and characterization of MS5 from Arabidopsis: A gene critical in male meiosis. *Plant J.* **15**, 345–356 (1998).
39. Cifuentes, M. *et al.* TDM1 Regulation Determines the Number of Meiotic Divisions. *PLoS Genet.* **12**, (2016).

40. Kawa, D. *et al.* SnRK2 Protein Kinases and mRNA Decapping Machinery Control Root Development and Response to Salt. *Plant Physiol.* **182**, 361–377 (2020).
41. Fujii, H., Verslues, P. E. & Zhu, J. K. Arabidopsis decuple mutant reveals the importance of SnRK2 kinases in osmotic stress responses in vivo. *Proc. Natl. Acad. Sci. U. S. A.* **108**, 1717–1722 (2011).
42. Cutler, S. R., Rodriguez, P. L., Finkelstein, R. R. & Abrams, S. R. Abscisic Acid: Emergence of a Core Signaling Network. *Annu. Rev. Plant Biol.* **61**, 651–679 (2010).
43. Williams, M. E. *et al.* Mutations in the Arabidopsis phosphoinositide phosphatase gene SAC9 lead to overaccumulation of PtdIns(4,5)P2 and constitutive expression of the stress-response pathway. *Plant Physiology* vol. 138 686–700 (2005).
44. Kunz, H. H. *et al.* Plastidial transporters KEA1, -2, and -3 are essential for chloroplast osmoregulation, integrity, and pH regulation in Arabidopsis. *Proc. Natl. Acad. Sci. U. S. A.* **111**, 7480–7485 (2014).
45. Stephan, A. B., Kunz, H. H., Yang, E. & Schroeder, J. I. Rapid hyperosmotic-induced Ca2+ responses in Arabidopsis thaliana exhibit sensory potentiation and involvement of plastidial KEA transporters. *Proc. Natl. Acad. Sci. U. S. A.* **113**, E5242–E5249 (2016).
46. Colmenero-Flores, J. M. *et al.* Identification and functional characterization of cation-chloride cotransporters in plants. *Plant J.* **50**, 278–292 (2007).
47. Bulankova, P., Riehs-Kearnan, N., Nowack, M. K., Schnittger, A. & Riha, K. Meiotic progression in Arabidopsis is governed by complex regulatory interactions between SMG7, TDM1, and the meiosis I-specific cyclin TAM. *Plant Cell* **22**, 3791–3803 (2010).
48. Szklarczyk, D. *et al.* STRING v10: Protein-protein interaction networks, integrated over the tree of life. *Nucleic Acids Res.* **43**, D447–D452 (2015).
49. Seppey, M., Manni, M. & Zdobnov, E. M. BUSCO: Assessing genome assembly and annotation completeness. in *Methods in Molecular Biology* vol. 1962 227–245 (2019).
50. Spalding, J. B. & Lammers, P. J. BLAST Filter and GraphicAlign: Rule-based formation and analysis of sets of related DNA and protein sequences. *Nucleic Acids Res.* **32**, (2004).
51. Marçais, G. *et al.* MUMmer4: A fast and versatile genome alignment system. *PLoS Comput. Biol.* **14**, (2018).
52. Stanke, M. & Waack, S. Gene prediction with a hidden Markov model and a new intron submodel. in *Bioinformatics* vol. 19 (2003).
53. Quevillon, E. *et al.* InterProScan: Protein domains identifier. *Nucleic Acids Res.* **33**, (2005).
54. Conesa, A. & Götz, S. Blast2GO: A comprehensive suite for functional analysis in plant genomics. *Int. J. Plant Genomics* **2008**, (2008).
55. D.M., E. & S., K. OrthoFinder2: fast and accurate phylogenomic orthology analysis from gene sequences. *bioRxiv* 466201 (2018) doi:10.1101/466201.
56. Martin, M. Cutadapt removes adapter sequences from high-throughput sequencing reads. *EMBnet.journal* **17**, 10 (2011).
57. Joshi, N. & Fass, J. Sickle: A sliding-window, adaptive, quality-based trimming tool for FastQ files (Version 1.33) [Software]. *Available at https://github.com/najoshi/sickle.* 2011 (2011).
58. Li, H. *et al.* The Sequence Alignment/Map format and SAMtools. *Bioinformatics* **25**, 2078–2079 (2009).
59. Li, H. & Durbin, R. Fast and accurate short read alignment with Burrows-Wheeler transform. *Bioinformatics* **25**, 1754–1760 (2009).
60. Broad Institute. Picard Tools - By Broad Institute. *Github* (2009).
61. McKenna, A. *et al.* The genome analysis toolkit: A MapReduce framework for analyzing next-

generation DNA sequencing data. *Genome Res.* **20**, 1297–1303 (2010).

62. Garrison, E. & Marth, G. Haplotype-based variant detection from short-read sequencing. (2012).
63. Narasimhan, V. *et al.* BCFtools/RoH: A hidden Markov model approach for detecting autozygosity from next-generation sequencing data. *Bioinformatics* (2016) doi:10.1093/bioinformatics/btw044.
64. Nei, M. Genetic Distance between Populations. *Am. Nat.* (1972) doi:10.1086/282771.
65. Anand, S. *et al.* Next generation sequencing of pooled samples: Guideline for variants' filtering. *Sci. Rep.* **6**, (2016).
66. Jombart, T. & Ahmed, I. adegenet 1.3-1: New tools for the analysis of genome-wide SNP data. *Bioinformatics* **27**, 3070–3071 (2011).
67. Venturini, L., Caim, S., Kaithakottil, G. G., Mapleson, D. L. & Swarbreck, D. Leveraging multiple transcriptome assembly methods for improved gene structure annotation. *Gigascience* **7**, (2018).
68. Cingolani, P. *et al.* A program for annotating and predicting the effects of single nucleotide polymorphisms, SnpEff: SNPs in the genome of Drosophila melanogaster strain w1118; iso-2; iso-3. *Fly (Austin).* **6**, 80–92 (2012).
69. Alexa, A. & Rahnenführer, J. Gene set enrichment analysis with topGO. *Bioconductor Improv.* (2007).
70. Smedley, D. *et al.* BioMart - Biological queries made easy. *BMC Genomics* (2009) doi:10.1186/1471-2164-10-22.
71. Grossmann, S., Bauer, S., Robinson, P. N. & Vingron, M. Improved detection of overrepresentation of Gene-Ontology annotations with parent-child analysis. *Bioinformatics* **23**, 3024–3031 (2007).
72. R Development Core Team, R. *R: A Language and Environment for Statistical Computing*. *R Foundation for Statistical Computing* vol. 1 (2011).

Supplemental Information

Table S1. GPS coordinates of population localities.

Table S2. Mean depth of coverage (MDOC) per pool of individuals from each population.

Table S3. Genes in the top 1% of Fst scores (1000 bp windows) in *C. amara*. Note: red lines denote six genes which are candidates also in *A. arenosa.*

Table S4. GO terms enriched in *C. amara* WGD candidate genes. Annotated: # genes in the GO category, Significant: # candidate genes in each category, p-values crom Fisher's exact test ('elim' method).

Table S5. Top 1% of amino acid substitutions with the highest fineMAV score.

Table S6. Genes in the top 1% of Fst scores (1000 bp windows) in *A. arenosa*.

Table S7. GO terms enriched in *A. arenosa* WGD candidate genes. Annotated: # genes in the GO category, Significant: # candidate genes in each category, p-values crom Fisher's exact test ('elim' method).

Table S8. Targeted search for patterns suggesting directional selection in *C. amara* ortologs of candidate *A. arenosa* meiosis genes.

Table S9. *C. amara* candidate genes that have more than one associated protein among *A. arenosa* candidates.

Table S10. Quality checks of DNA isolated from LUZ.

Table S11. An assessment of genome completeness using BUSCO.

Supplemental Figures

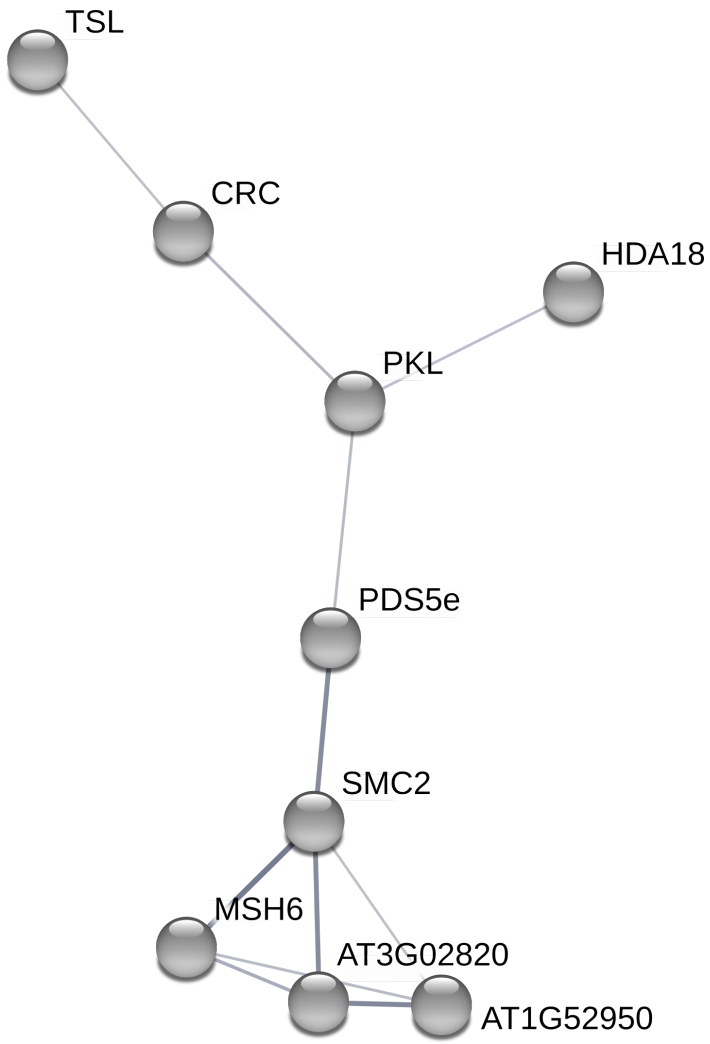

Figure S1: *C. amara* candidate meiosis gene associations as identified by STRING. We used only medium confidence associations and higher (shown as thickness of lines connecting genes).

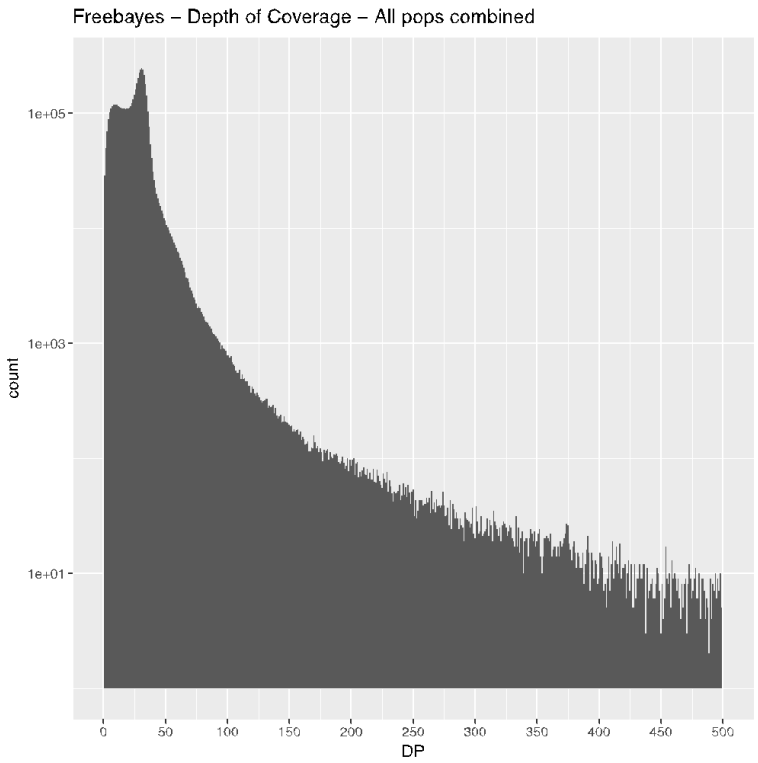

Figure S2: Distribution of read depth over all sequenced samples

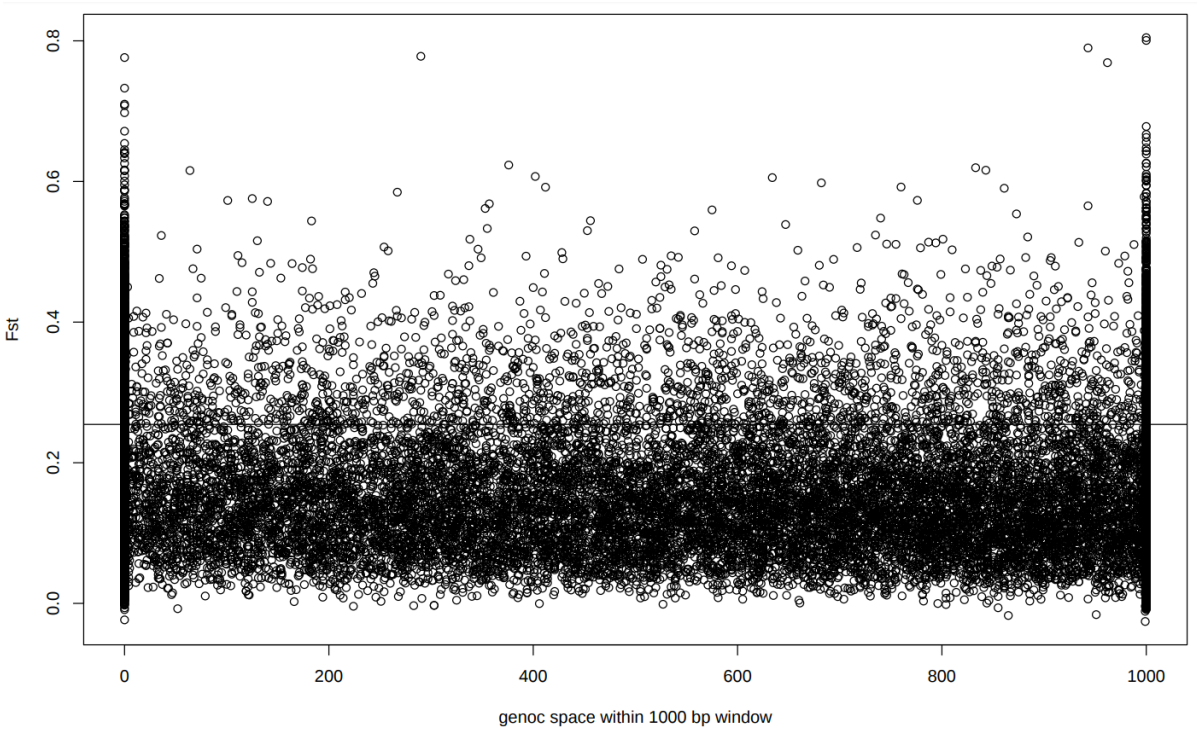

Figure S3: Relationship between the proportion of genic space within a window and Fst